A molecular perspective on the cleaning of oil paintings

Baij, C.L.M.

Publication date
2020
Document Version
Other version
License
Other

CHAPTER

THREE

FATTY ACID DIFFUSION AND THE FORMATION OF METAL SOAPS IN OIL PAINT MODEL SYSTEMS

Parts of this chapter are published in:

L. Baij,* J. J. Hermans,* K. Keune and P. Iedema, Time-Dependent ATR-FTIR Spectroscopic Studies on Fatty Acid Diffusion and the Formation of Metal Soaps in Oil Paint Model Systems, *Angewandte Chemie Internation Edition*, **2018**, 57, 7351–7354.

*equal contribution

3.1 Introduction

Traditional oil paints are a mixture of mainly inorganic pigments, a drying oil (triglycerides with a high degree of unsaturation) and a wide variety of possible additives. As the oil binding medium dries and ages through autoxidation reactions, this mixture becomes a complex heterogeneous system of solid particles suspended in a dense polymer matrix. Oil paints are subject to slow deterioration processes that affect the appearance and structural integrity of oil paintings. Factors such as humidity,[99,100] exposure to solvents,[28,68] temperature changes and exposure to light[101] are known to influence the stability of oil paint. Reactions between pigments or metal-based siccatives and the oil binder can lead to the prominent conservation issue of *metal soap* formation: complexes of metal ions (usually lead or zinc) and long-chain saturated fatty acids (SFAs). These complexes can form large crystalline aggregates that protrude through the paint surface and have been associated to cases of brittleness, transparency and delamination in oil paint layers.[3]

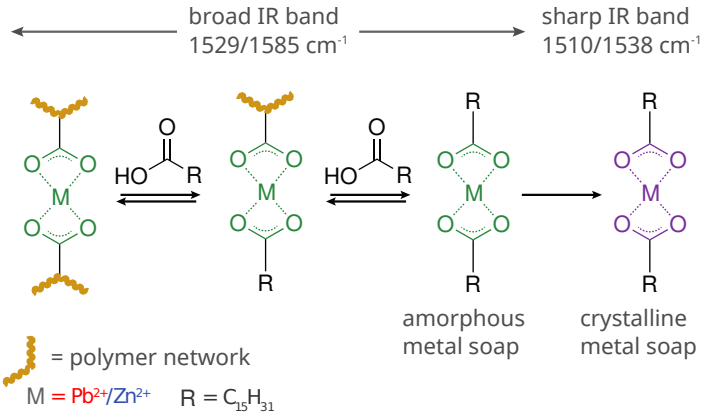

Scheme 3.1 Hypothetical pathway for the formation of crystalline metal soaps from ionomeric binding media upon exposure to palmitic acid (HPa).[2] The noted wavenumbers refer to the position of the $\nu_a COO^-$ vibration band for lead (red) and zinc (blue) complexes. The geometry of the metal carboxylate complexes is depicted schematically.

An important discovery has been that metal ions (originating from pigments or driers) migrate into the binding medium, where they are distributed throughout the polymerised oil network and associated to carboxylate groups.[2,42,43] Such an *ionomer* medium contains clusters of metal carboxylate groups (identified by a broad ν_a COO^- band in infrared (IR) spectra) that, while potentially reactive towards long-chain saturated fatty acids (SFAs), could contribute to the stability of the oil network on the short term.[43] SFAs can either be formed by partial hydrolysis of the polymerised oil network, or be derived from paint additives such as aluminium stearate.[102] Our current hypothesis, illustrated in Scheme 3.1, is that the presence of free SFAs leads to the formation of amorphous metal soap complexes. Subsequently, due to the low solubility of metal soaps in oil,[77] these complexes will tend

to crystallise and form metal soap aggregates. With FTIR spectroscopy, this crystalline state of metal soaps can be distinguished from amorphous metal carboxylate species by their sharp COO^- bands at 1510 cm^{-1} (Pb) or 1538 cm^{-1} (Zn).

Linseed oil-based ionomer model systems, time-dependent ATR-FTIR spectroscopy and ATR-FTIR imaging were used to investigate the diffusion of a SFA (palmitic acid, HPa) and its reaction with metal carboxylate clusters. ATR-FTIR spectroscopy has proven to be a powerful tool to study dynamic processes in polymer films.[32,49–52,103] Mature oil paint 'model' systems (**Znpol** and **Pbpol**) were synthesised by co-polymerisation of linseed oil (LO) and metal sorbate (2,4-hexadienoate) at 150 °C (see Experimental). We have proven that these systems are representative of mature oil paint in terms of metal carboxylate concentration and structure.[2,42,43] The paint models were either subjected to fatty acids in solution or to molten fatty acids, because long-chain fatty acids are solids at room temperature. Both conditions entail a departure from the 'real' conditions in oil paintings to some degree but *do* allow studying essential reaction-diffusion processes.

3.2 Results and Discussion

3.2.1 Time-dependent ATR-FTIR studies of metal soap formation

The model systems were exposed to a solution of HPa in acetone in a custom ATR sample cell (Figure 3.13) that ensured a constant contact between the samples and the ATR crystal. These experiments provided information on the sequence of several diffusion and reaction processes that happen on much longer timescales in real oil paintings.

Figure 3.1 shows the evolution of IR spectra of **Znpol** and **Pbpol** recorded during the first 200 minutes of exposure to a solution of HPa in acetone. The spectra before exposure exhibit clear amorphous metal carboxylate bands in the 1500–1650 cm^{-1} region. At $t > 0$, IR bands corresponding to acetone appeared within minutes, while the remainder of the spectrum decreased in intensity due to a decreasing concentration of polymer in the measurement volume. After 10–20 minutes, carboxylate bands associated with crystalline lead palmitate ($PbPa_2$) and zinc palmitate ($ZnPa_2$) were detected. In **Pbpol**, CH_2 progression bands between 1240–1340 cm^{-1}, associated with packed all-*trans* alkyl chains, were clearly visible. Figure 3.2 shows X-ray diffraction measurements on ionomer films after exposure to HPa solution that confirm the attribution of the sharp $\nu_a COO^-$ bands appearing in Figure 3.1 to crystalline metal palmitate (MPa_2) complexes.

Integrated band areas corresponding to acetone, $PbPa_2$ and $ZnPa_2$ are shown in Figure 3.3, which clearly illustrate the sequence of diffusing species detected at the bottom of the film. To obtain accurate areas of the crystalline MPa_2 bands, a custom spectral processing algorithm was applied to subtract contribution of the overlapping broad metal carboxylate band (see Figure 3.14 for details). After 30 minutes, the concentration of acetone reached a constant value in the measurement volume (penetration depth[45] d_p varies

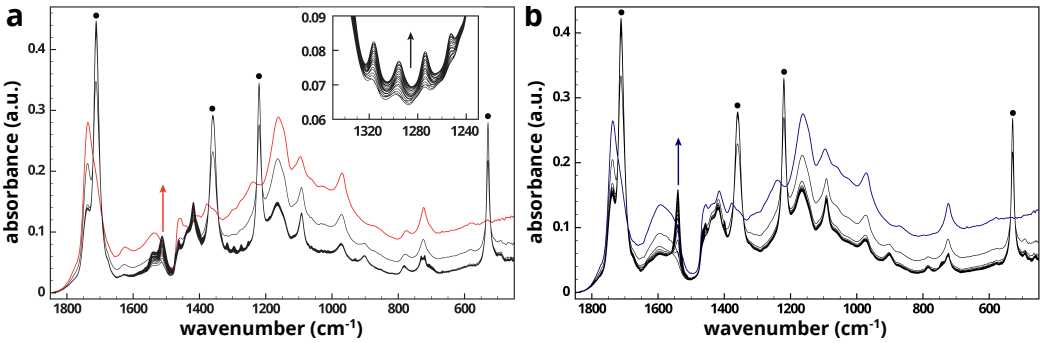

Figure 3.1 A baseline-corrected selection of IR spectra with 10 min time intervals of **a Pbpol** and **b Znpol** ionomers of 140–160 μm thickness, recorded during the first 200 minutes of exposure to a solution of HPa in acetone. Spectra at $t = 0$ are highlighted in red and blue for lead and zinc, respectively. Bands associated with acetone are marked by ●. Arrows indicate the $\nu_a COO^-$ vibration of crystalline MPa_2 complexes. The inset in **a** shows the CH_2 progression bands of $PbPa_2$.

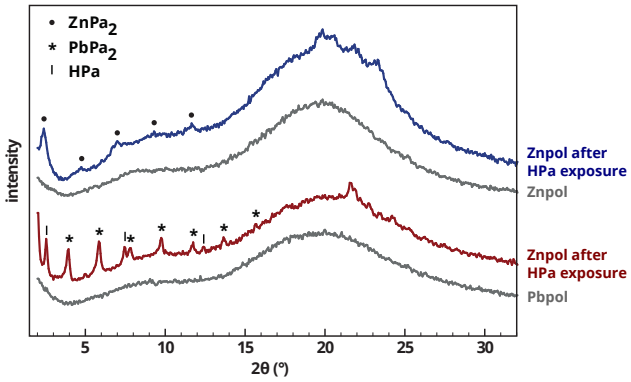

Figure 3.2 XRD traces of Pbpol and Znpol ionomer films before and after exposure to a solution of HPa in acetone. In both cases, the samples show characteristic long spacing peaks corresponding to crystalline zinc and lead palmitate.[104] Pbpol also shows peaks of HPa that crystallised after remaining traces of the acetone solution evaporated.

from 0.5 to 3.5 μm from 3500 to 500 cm^{-1}). IR bands of $PbPa_2$ and $ZnPa_2$ were detected just minutes after acetone was first observed. The shape of the profiles and the time at which species are first detected (delay time τ_d) give valuable information on the reaction and diffusion processes taking place. Additionally, because the initial broad COO^- band area was nearly constant ($\sigma = 6\%$ in a set of 10 repeats), differences in absolute band areas within the series can be used to measure MPa_2 concentrations qualitatively.

To investigate the effect of the presence of metal ions on HPa diffusion, we compared reactive and unreactive films (*i.e.* linseed oil without metal ions). Films of pure polymerised linseed oil **pLO** were exposed to molten HPa at 70 °C while monitoring the ν_a COOH band at 1710 cm^{-1} (see Figure 3.14 for the integration method). The diffusion

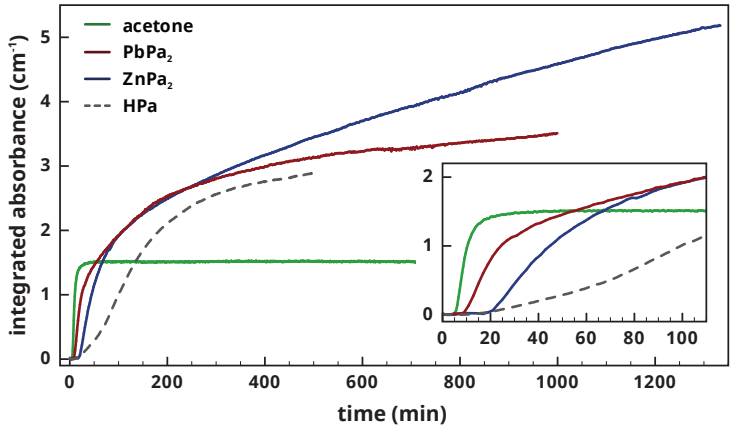

Figure 3.3 Profiles of IR band areas corresponding to acetone (529 cm^{-1}), $PbPa_2$ (1510 cm^{-1}), and $ZnPa_2$ (1538 cm^{-1}) in **Pbpol** and **Znpol** ionomers during exposure to a solution of HPa in acetone (56 mM). The diffusion profile of molten HPa (1710 cm^{-1})was recorded at 70 °C in a polymerised linseed oil film (**pLO**).

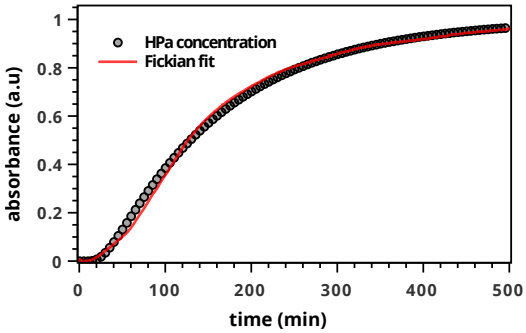

Figure 3.4 Integrated COOH band area of HPa during diffusion of molten HPa into a polymerised linseed oil film at 70 °C. The data was fitted to a Fickian diffusion model appropriate for the ATR-FTIR measurement geometry as described by Fieldson and Barbari.[45]

profile of molten HPa was described well with a simple Fickian diffusion model,[45] yielding a diffusion coefficient $D = 1.15 \cdot 10^{-8}$ cm^2/s (Figure 3.4).

The fast formation of MPa_2 complexes in the measurement volume demonstrates that metal soap crystallisation starts directly after HPa reaches the bottom of the film, indicating that the presence of free SFAs in ionomeric binding media is enough to cause spontaneous metal soap crystallisation. Consequently, any process that may increase the free SFA concentration in a paint (ester hydrolysis, wax-resin lining of paintings,[16] etc.), is expected to have a significant effect on the metal soap formation rate. Comparing the profiles of **Pbpol** and **Znpol** (Figure 3.3), $PbPa_2$ had a τ_d of approximately 10 min, while for $ZnPa_2$ $\tau_d = 20$ min. Interestingly, τ_d for molten HPa in the unreactive **pLO** was much

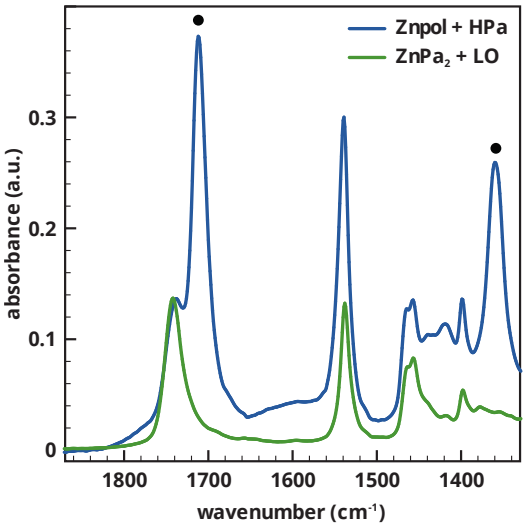

Figure 3.5 FTIR spectra of (blue) Znpol ionomer after reaction with a HPa solution for 24 hours and (green) of a homogeneous suspension of $ZnPa_2$ and linseed oil. The latter sample contained the same ratio of metal-carboxylate bonds to ester bonds (COOM/COOR) as the initial unreacted Znpol ionomer film. The spectra were normalised on the maximum of the ester carbonyl vibration at 1740 cm^{-1} to allow a comparison of the concentration of other molecular species relative to the concentration of ester groups. The fact that the asymmetric carboxylate stretch vibration at 1538 cm^{-1} is so much more intense in the Znpol sample than in the mixture of $ZnPa_2$ suggests that there is a gradient in the concentration of $ZnPa_2$ in Znpol towards the bottom of the film after reaction with HPa solution. In other words, $ZnPa_2$ seems to exhibit preferred crystallisation at the bottom of the film. Bands associated with acetone are marked by ●.

smaller than the delay time of crystalline MPa_2 complexes in reactive ionomer systems. This observation indicates that the initial HPa diffusion rate is strongly increased by the simultaneous flow of acetone in the same direction. Moreover, the MPa_2 concentration profile keeps increasing slowly on long timescales, unlike the diffusion profiles of acetone or other solvents.[32]

The observed concentration profiles offer a better understanding of the reaction and diffusion of free SFAs, solvents (cleaning agents) as well as the possible transport of network-bound metal ions in oil paintings. The idea that the measurement system contains multiple diffusion processes seems to be confirmed by the presence of a fast and slow regime (Figure 3.3). One explanation for these two regimes is a decreasing HPa diffusion rate as the local concentration of crystalline MPa_2 increases and fills up the free volume in the polymer network. Alternatively, if there is a slow migration process of metal ions at play, the fast regime of MPa_2 crystallisation can be interpreted as the consumption of network-bound metal carboxylates initially present in the measurement volume. The slow regime would then be caused by M^{2+} migration, causing crystalline metal soaps to keep forming at the bottom of the sample even when the initial concentration of metal ions

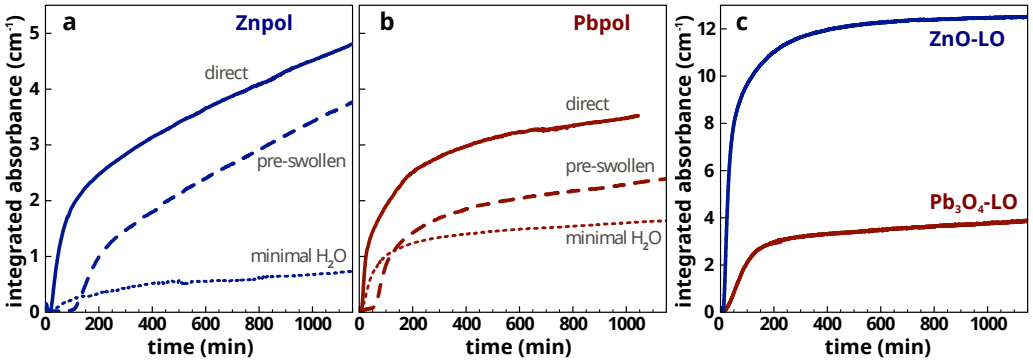

Figure 3.6 MPa_2 concentration profiles in **a Znpol** and **b Pbpol** ionomers, comparing experiments with direct exposure to a HPa solution (solid), pre-swelling with acetone (dashed) or removal of most of the water in the system (dotted). The pre-swollen curves were shifted horizontally to place $t = 0$ at the moment of HPa addition. **c** MPa_2 profiles in paint films pigmented with ZnO (blue curve) or Pb_3O_4 (red curve).

in the measurement volume has been consumed. In this scenario, metal soaps would need to show preferential crystallisation near the polymer/ATR-crystal interface. Such an accumulation process is also suggested by the intensity of the $ZnPa_2$ band in films after long exposure to HPa solutions (Figure 3.5). The intensity of this band is far greater in **Znpol** after reaction than in a mixture of $ZnPa_2$ and linseed oil with the same Zn^{2+} concentration. Interestingly, even though one would expect metal ions to migrate towards the *top* of the film (where HPa arrives first), these measurements suggest that M^{2+} ions from outside the measurement volume have migrated towards the *bottom* of the film instead.

The effect of acetone flow on the diffusion of HPa was investigated by carrying out reaction-diffusion experiments in which HPa was only introduced after the sample film was first fully saturated with acetone (Figure 3.6a and b). While the MPa_2 profile shape was unaffected, the pre-swollen films *did* show a significantly increased τ_d. This delay supports the notion that the rapid initial diffusion of HPa and subsequent crystallisation of MPa_2 shown in Figure 3.3 is indeed caused by the initial acetone flow. In all experiments, τ_d was approximately twice as long in **Znpol** compared to **Pbpol**. Previous research demonstrated that crystallisation from the melt is a faster process for $PbPa_2$ than for $ZnPa_2$,[77] which offers an explanation for the earlier detection of $PbPa_2$. Significant differences in the diffusion rate of HPa in the two ionomers are not expected, because the diffusion constants of a wide range of solvents were approximately equal in **Znpol** and **Pbpol** (see CHAPTER 2).[32]

In studies of oil paint ageing, water has always been suspected of causing a broad range of degradation phenomena, primarily through hydrolysis of the triacylglyceride ester bonds. We studied the effect of water on the reaction-diffusion processes by removing as much water from the system as possible. The dotted curves in Figure 3.6a and b show

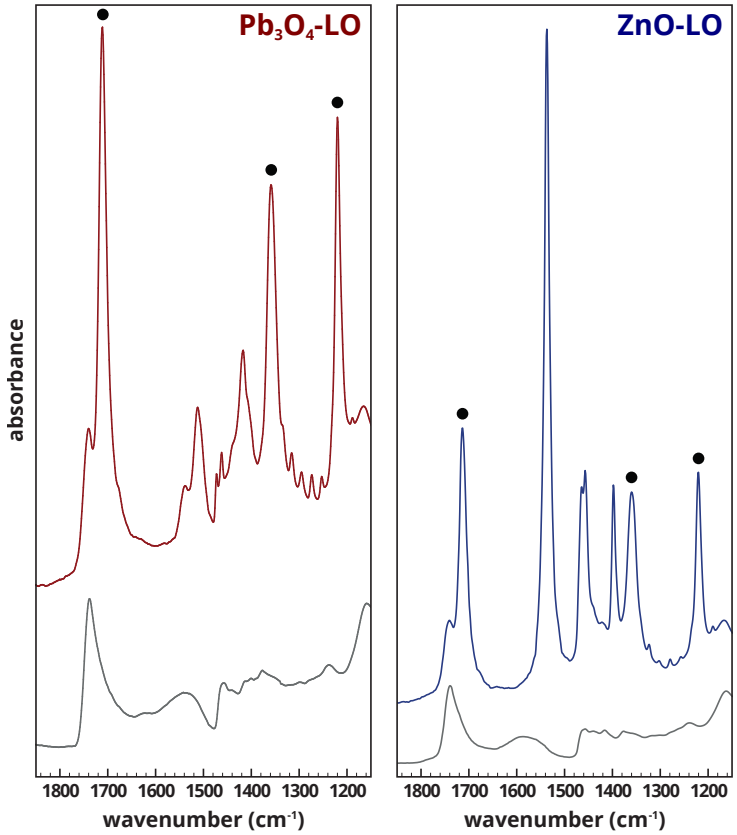

Figure 3.7 ATR-FTIR spectra of Pb_3O_4-LO and ZnO-LO model paint films before (bottom) and after (top) reaction with a solution of HPa in acetone. Note the broad ionomer metal carboxylate band in the spectra at t = 0, and the high intensity of the crystalline metal carboxylate band of the metal palmitates (1510 cm^{-1} and 1538 cm^{-1} for lead and zinc, respectively) compared to the ester carbonyl band at 1738 cm^{-1}. Spectra were normalised to the maximum of the ester carbonyl band at 1738 cm^{-1} and vertically shifted for clarity. Bands associated with acetone are marked with •.

the MPa_2 profiles recorded on films that were dried overnight in vacuum at 100 °C, using dry acetone that was freshly distilled over B_2O_3. Both for **Znpol** and **Pbpol**, τ_d was similar to the non-dried runs. However, the subsequent rate of MPa_2 formation was slower and the final conversion was much lower, especially for **Znpol**. This result demonstrates that even low concentrations of water in the system have a profound effect on the rate of metal soap formation. Rather then promoting metal soap formation by generation of free SFAs through ester hydrolysis, here water increases the rate of MPa_2 formation when free SFAs are introduced to the system. We hypothesise that water lowers the activation energy for metal ion transfer between carboxylate groups, thereby increasing the metal ion migration rate through the polymer network and the consumption of metal ions by free SFAs. Such an effect has been demonstrated in perfluorosulfonated ionomer membranes.[105]

We compared the unpigmented ionomer systems **Znpol** and **Pbpol** with complete paint models consisting of zinc oxide (ZnO) or minium (Pb_3O_4) in linseed oil, dried at 60 °C for one week (denoted **ZnO-LO** and **Pb_3O_4-LO**, respectively). Both these paint models showed broad COO^- bands in FTIR spectra nearly identical in both shape and intensity to **Znpol** and **Pbpol** systems (Figure 3.7, bottom), indicating the formation of ionomeric binding medium.[43] Figure 3.6c shows the crystalline MPa_2 profiles for **ZnO-LO** and **Pb_3O_4-LO** during exposure to HPa solution. The pigmented films showed very fast MPa_2 crystallisation on short timescales. The concentration of $ZnPa_2$ in the **ZnO-LO** system reached a constant level after approximately 600 minutes, while the concentration of $PbPa_2$ was still increasing in the **Pbpol** system after 1000 minutes.

It is apparent that pigmentation strongly affects the metal soap formation process. Though the intensities of the initial broad COO^- bands in **ZnO-LO** and **Pb_3O_4-LO** were highly similar to those in **Znpol** and **Pbpol**, the initial slope of the profiles and the band intensities after 1000 minutes were, especially in the case of **ZnO-LO**, much greater in the case of pigmented films (compare Figure 3.6a, b and c). Two effects can explain these differences. Firstly, in the case of **ZnO-LO**, it is likely that ZnO particles are consumed as the total concentration of COOH groups increases when HPa flows into the system and metal soaps form. Secondly, the pigment surface could act as a suitable nucleation site for MPa_2. It is conceivable that both factors are in effect to different degrees in **Pb_3O_4-LO** and **ZnO-LO**, explaining the differences in their profile shapes. If Pb_3O_4 is less prone to degradation than ZnO, this higher stability could result in a slower release of Pb^{2+} during the measurement and an overall profile shape that is largely governed by slow transport of Pb^{2+} ions that were already present in the binding medium at the start of the experiment.

3.2.2 ATR-FTIR imaging of zinc soap products in cross-sections

The influence of ZnO particle size and concentration on zinc soap formation

Since time-dependent ATR-FTIR measures only the bottom of the films and does not provide information on the distribution of zinc soap products, it was decided to use ATR-FTIR imaging on embedded cross-sections.[106] After HPa exposure, the models systems were embedded and measured in order to study potential pigment degradation or metal ion migration.

First, we tested the hypothesis that ZnO particles are consumed during the experiment by exposing mixed ZnO/TiO_2 paint models with increasing ZnO concentrations (**ZnO-TiO_2-LO**) to HPa in acetone. After 24 hours of exposure to HPa in acetone, the embedded cross sections were imaged. Figure 3.8a shows ATR-FTIR heat maps of the crystalline $ZnPa_2$ band at 1538 cm^{-1}, showing an increasingly intense $ZnPa_2$ band for increasing ZnO concentrations and confirming the formation of more zinc soaps when more ZnO is present (compare *e.g.* heat maps for 2 wt% and 80 wt% ZnO in Figure 3.8a). Figure 3.8b shows a selection of ester normalised FTIR spectra extracted from the maps. The spectra

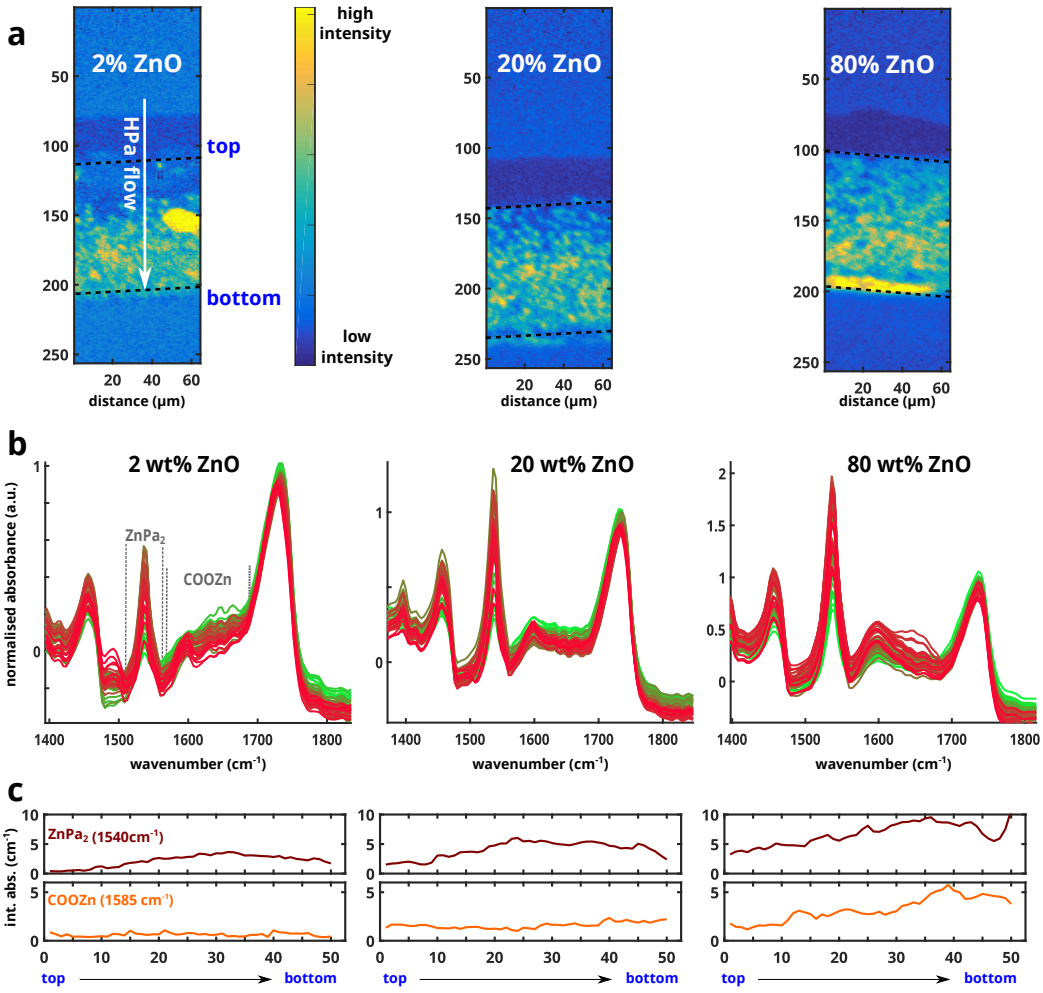

Figure 3.8 **a**: Ester normalised heat maps of the $ZnPa_2$ band (1540 cm^{-1}) after reaction of **ZnO-TiO_2-LO** samples (2–80 wt% ZnO) with a solution of HPa in acetone (direction of HPa flow indicated with arrow). Spherical high intensity spot in the left image and thin layer at the bottom interface in the right image are caused by protein contamination. **b**: Ester normalised imaging ATR-FTIR spectra inside the **ZnO-TiO_2-LO** layer after HPa exposure. The layer was divided in 50 slabs, spectra were averaged over each slab and plotted as a function of depth (position inside the layer). Green corresponds to the top, red to the bottom of the layer. Areas with protein contamination were omitted. **c**: Relative concentration profiles obtained by integration of the $ZnPa_2$ band and the amorphous zinc carboxylate band (COOZn, centered at 1585 cm^{-1} and integrated between 1560–1700 cm^{-1} as indicated with dashed lines) along the depth of the films. Upon increasing the ZnO concentration from 2–80 wt%, a clear increase in both $ZnPa_2$ and COOZn is observed.

were obtained by dividing the measured layer into 50 slabs, performing averaging along the slabs and plotting the average spectra for all 50 slab positions between top and bottom. In Figure 3.8b, green corresponds to the top, red to the bottom of the imaged

layer. Subsequent integration of the $ZnPa_2$ band and the amorphous zinc carboxylate band (COOZn, 1585 cm^{-1}) along the depth of the films yields the relative concentration profiles that are displayed in Figure 3.8c. We note that the amorphous zinc carboxylate band shows interesting variations in intensity and peak position (see CHAPTER 5), but we here only consider the total intensity in this region of the spectrum as a measure of the amount of amorphous zinc carboxylates. Moreover, minor contributions from a small band around 1600 cm^{-1} caused by the Technovit embedding resin may lead to a slight overestimation of the total band intensity, but integration of this spectral region gives access to interesting information on the relative concentration and spatial distribution of amorphous zinc carboxylates nevertheless. It can be seen in Figure 3.8b and c that for higher ZnO concentrations, an increase in *both* the $ZnPa_2$ and the COOZn band are observed. Zinc ions (originating from ZnO particles) thus associate to carboxylate groups to refill the ionomer network and increase the amount of COOZn. In addition, more crystalline zinc soaps are formed when higher ZnO concentrations are present. These results shows that an important mechanism in zinc soap crystallisation is filling the network with amorphous COOZn, followed by a crystallisation step (see Scheme 3.1). Since the IR bands associated with amorphous COOZn containing alkyl chains that are linked to the polymer network, or disordered as in molten $ZnPa_2$ (CHAPTER 5), are fundamentally indistinguishable, we can not discriminate between these two situations. As a result, the increasing formation of COOZn upon increasing the amount of ZnO (Figure 3.8b and c) may be partly explained by the presence of $ZnPa_2$ molecules that have not yet crystallised. Therefore, it can not be excluded that some HPa reacts directly with ZnO at the ZnO surface to form crystalline $ZnPa_2$ without an intermediate exchange step with COOH groups attached to the polymer network.

To further investigate the breakdown of ZnO, we explored the effects of particle size on the formation of $ZnPa_2$ by using ZnO with a <100 nm particle size (100 wt% ZnO, sample designated **nanoZnO-LO**), resulting in a strong increase in ZnO surface area. It was hypothesised that, upon increasing the ZnO surface area, the release of zinc ions into the network would be facilitated, resulting in an increase in either $ZnPa_2$ or COOZn, or both. Figure 3.9b shows a selection of IR spectra taken from a cross-section of a **nanoZnO-LO** model system after 24 hours of exposure to HPa in acetone. Comparing Figure 3.9b with spectra from Figure 3.8b, it is clear that both the formation of $ZnPa_2$ and amorphous COOZn increased strongly when nano ZnO is used. This observation is further illustrated by the relative concentration profiles for $ZnPa_2$ and COOZn that are displayed in Figure 3.9c, showing an almost twofold increase in amorphous COOZn formation compared to normal ZnO. These results further demonstrate that (1) ZnO particles are actively broken down during the experiment and (2) highlight that the reaction of free SFAs with Zn^{2+} ions incorporated in the ionomer network is an important pathway in crystalline $ZnPa_2$ formation. Although on the basis of these experiments it can not be excluded that HPa also reacts directly with ZnO directly at the ZnO surface, the results

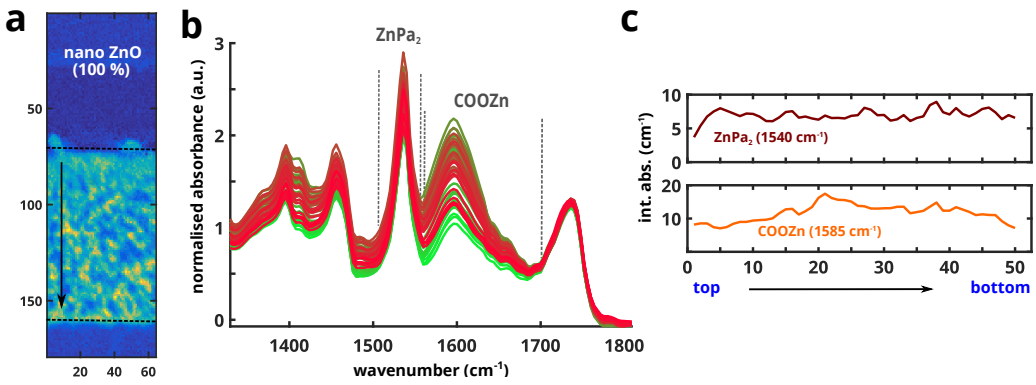

Figure 3.9 **a**: Ester normalised heat maps of the $ZnPa_2$ band (1540 cm^{-1}) after reaction of the **nanoZnO-LO** sample (100 wt% nano ZnO) with a solution of HPa in acetone (direction of HPa flow indicated with arrow). **b**: Ester normalised imaging ATR-FTIR spectra inside the **nanoZnO-LO** layer after HPa exposure. The layer was divided in 50 slabs (slices), spectra were averaged over each slab and plotted as a function of depth (position inside the layer). Green corresponds to the top, red to the bottom of the layer. **c**: Relative concentration profiles obtained by integration of the $ZnPa_2$ band and the amorphous zinc carboxylate band (COOZn, centered at 1585 cm^{-1} and integrated between 1560–1700 cm^{-1} as indicated with dashed lines) along the depth of the films. The use of nano ZnO shows a strong increase in the amount of $ZnPa_2$ and COOZn, as compared to regular ZnO (Figure 3.8b and c).

verify that unpigmented binding medium model systems are valuable tools for studying metal soap crystallisation.

The influence of pigmentation on the spatial distribution of zinc soaps

The important role of the ionomeric binding medium in metal soap formation has been illustrated above. However, the fact the that bottom of the films contained much more zinc soaps than the top (Figure 3.5) proves that zinc ions must have migrated during the experiment with HPa in acetone. To investigate this phenomenon in more detail, cross-sections were taken at timed intervals during the experiments with **Znpol** and direct exposure to HPa in acetone (see Figure 3.6a and b, direct exposure).

Cross-sections were taken at 30, 60, 120 minutes, 24 hours and 67 hours, embedded in Technovit resin, polished and measured using ATR-FTIR imaging. The results are shown in Figure 3.10, showing preferential $ZnPa_2$ formation in the direction opposite to the HPa flow (at the interface of the ATR crystal). At present, the reason for this preferential crystallisation at the ATR-interface (from now on *interface effect*) is unclear. Due to the lack of suitable nucleation sites for crystallisation inside unpigmented **Znpol** ionomers, the most suitable nucleation site may be the ATR crystal itself. However, attempts to eliminate the interface effect using amorphous substrates such as polymerised linseed oil or PET also showed the interface effect, suggesting that the crystallinity of the ATR crystal

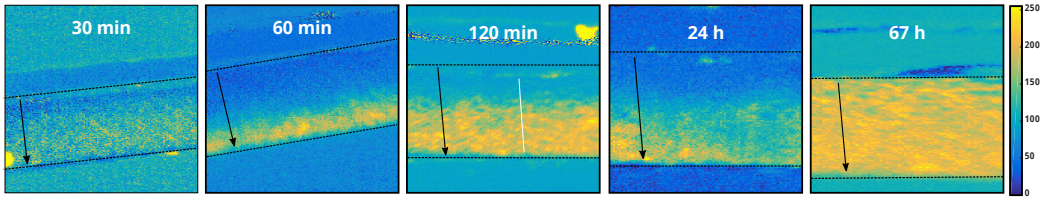

Figure 3.10 Ester normalised heat maps of the $ZnPa_2$ band (1540 cm^{-1}) after reaction of a **Znpol** sample with a solution of HPa in acetone for 30, 60, 120 minutes, 24 hours and 67 hours. Direction of HPa flow indicated with arrow. The maps clearly show preferential $ZnPa_2$ formation in the opposite direction of the HPa flow (at the interface of the ATR crystal). Spherical high-intensity spots (visible in samples taken at 30 and 120 min) are caused by protein contamination.

does not play an important role. It was also hypothesised that in absence of pigment, the relative rates of HPa diffusion and $ZnPa_2$ formation might cause crystallisation to start at a specific depth that corresponds to the thickness of the films used, and therefore result in the formation of $ZnPa_2$ at the bottom of the films. Experiments on thicker films (> 300 μm) did not confirm this hypothesis and showed the interface effect nevertheless. It is important to note that, despite the interface effect, the measured trends in crystallisation rate and effects of solvents and water on MPa_2 formation in ionomers remain valid.

The interface effect was not observed in experiments with reactive pigments such as ZnO or Pb_3O_4 (see *e.g.* Figure 3.8a). Besides being consumed upon HPa exposure, pigments may therefore play a role as nucleation sites for crystalline metal soap formation. To rule out the degradation of pigment particles and focus on the role of pigments during metal soap crystallisation, we investigated a **Znpol** ionomer filled with inert, coated, rutile TiO_2 pigment (**Znpol-TiO_2**). Such a 'filled' ionomer might provide additional insights in the origins of the interface effect.

Imaging ATR-FTIR heat maps of the $ZnPa_2$ band, taken on embedded cross-sections of a **Znpol-TiO_2** sample after HPa exposure for 15, 30, 60, 120 minutes and 24 hours are displayed in Figure 3.11. The heat maps clearly show that a relatively homogeneous $ZnPa_2$ distribution is present at all times. These results confirm that the presence of inert pigment particles strongly influence the dynamics of zinc soap crystallisation. Apart from influencing the distribution of $ZnPa_2$, an enhanced rate of $ZnPa_2$ formation for **Znpol-TiO_2** compared to **Znpol** was also found in time-dependent ATR-FTIR measurements (Figure 3.12). We can thus conclude that, although time-dependent ATR-FTIR measurements do not give information on the metal soap distribution, the trends observed in the rates of MPa formation (Figure 3.12) are, except for **nanoZnO-LO**, in agreement with imaging ATR-FTIR measurements. The fact that **nanoZnO-LO** does not show increased formation of zinc soaps compared to normal ZnO (Figure 3.12) at high concentrations, might be explained by the measured intensity of pure $ZnPa_2$, which is of similar magnitude to what is measured at the bottom of the films in these experiments. We note that the relevance

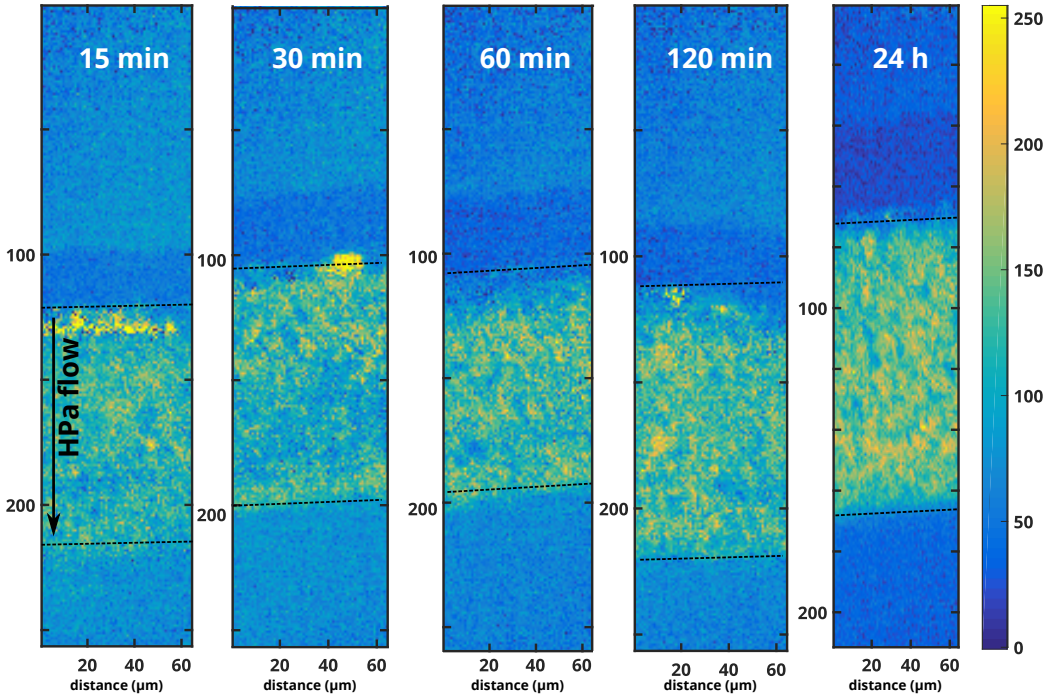

Figure 3.11 Ester normalised heat maps of the $ZnPa_2$ band (1540cm^{-1}) after reaction of a **Znpol-TiO_2** samples with a solution of HPa in acetone for 15, 30, 60, 120 minutes and 24 hours. Direction of HPa flow indicated with arrow. The maps clearly show homogeneous $ZnPa_2$ formation throughout the depth of the film.

of the measured interface effect for paintings conservation practice is currently unclear. Although the crystallisation of zinc soaps at interfaces is often observed in practice,[3,107] it remains to be seen if the presence or absence of (reactive) pigments is the cause of this phenomenon.

In summary, two combined effects of reactive ZnO pigments that enhance the rate and amount of $ZnPa_2$ formation can be distinguished:

- ZnO particles can break down during HPa exposure, either by the reaction of HPa directly at the ZnO surface or by providing zinc ions to empty carboxylic acid groups in the network. Since high concentrations of HPa are used, both ZnO breakdown pathways probably occur during our experiments.
- ZnO particles can serve as nucleation site for zinc soaps to crystallise, thereby enhancing the rate of nucleation, crystallisation, or both. Because inert TiO_2 particles showed this effect, it is likely that reactive ZnO particles will operate by the same mechanism.

The effects discussed here highlight the complexity of the metal soap crystallisation process

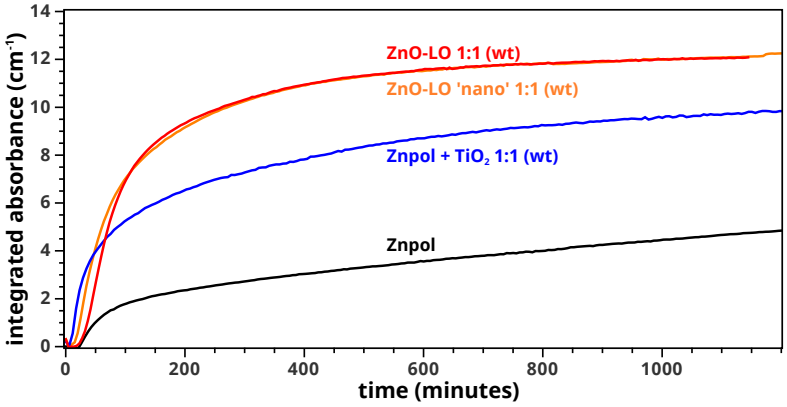

Figure 3.12 $ZnPa_2$ concentration profiles in **Znpol** and filled **Znpol-TiO_2** ionomers, **ZnO-LO** and **nanoZnO-LO** with direct exposure to a HPa solution. Except for **nanoZnO-LO** which does not show an increase compared to normal ZnO, the observed trends of $ZnPa_2$ formation over time (using time-dependent ATR-FTIR spectroscopy and measuring the bottom of the films) are in qualitative agreement with the information on the $ZnPa_2$ distribution obtained with ATR-FTIR imaging.

in paints and stress that time-dependent ATR-FTIR spectroscopy and imaging ATR-FTIR are powerful methods to study such complex processes with high chemical specificity.

3.3 Conclusions

We have described a time-dependent ATR-FTIR method using a custom sample cell and spectral processing algorithms that is capable of accurately monitoring complex reaction-diffusion processes in polymer media. Using this method, fast crystallisation of metal soaps was observed in ionomeric oil paint binding media model systems upon exposure to a solution of palmitic acid in acetone, showing that the availability of ionomeric metal carboxylates and free fatty acids is a sufficient condition for metal soap formation.

The transport rate of fatty acids through the binding medium is enhanced by solvent diffusion, which has important implications for the practice of solvent cleaning of paints with reactive molecules on their surface. Additionally, low concentrations of water or the presence of pigment particles in the films increase the rate of metal soap formation. It is found that reactive pigment particles can break down during metal soap formation and release metal ions into the binding medium. This phenomenon was studied in detail for reactive ZnO pigments and two combined effects were found: (1) ZnO particles can break down when exposed to SFAs, thus enhancing the rate and amount of $ZnPa_2$ formation and (2) pigment particles can serve as nucleation site for zinc soaps to crystallise, thereby enhancing the rate of nucleation, crystallisation, or both.

The reaction-diffusion experiments described here contribute to the understanding of the mechanisms that drive the formation of metal soap aggregates in oil paintings, and

highlight the potential of time-resolved ATR-FTIR spectroscopy and ATR-FTIR imaging for the study of dynamic processes in polymer films with high chemical specificity.

3.4 Experimental

Sample preparation Metal sorbate complexes were synthesised by dissolving 550 mg sorbic acid (Aldrich, 99+%) with 1 mL triethylamine (Sigma-Aldrich, >99%) in 20 mL demineralised water at 50 °C. The addition of 1.0 g $Zn(NO_3)_2 \cdot 6\,H_2O$ (Sigma-Aldrich p.a.) or 1.1 g $Pb(NO_3)_2$ (Sigma-Aldrich, >99 %) dissolved in 5 mL water resulted in immediate precipitation of the white product. After stirring for 20 minutes, the product was separated by vacuum filtration, washed with water followed by ethanol and acetone, and dried overnight under reduced pressure. The metal sorbate salts were stored under N_2 atmosphere to avoid oxidation.

Binding medium model systems **Znpol** and **Pbpol** were made by grinding 250 mg zinc sorbate or an equivalent molar amount of lead sorbate with 1750 mg cold-pressed untreated linseed oil (LO, Kremer Pigmente) to a smooth paste with mortar and pestle. The concentration of metal ions was equivalent to a molar metal carboxylate bond to triacylglyceride (TAG) ester ratio (COOM/COOR) in the uncured sample mixture of 0.29. This concentration corresponds to roughly 420 mM zinc in the polymer. The mixture was applied to 50 × 75 mm glass slides and spread with a draw-down bar to achieve a wet thickness of 190 μm. The layers were cured overnight in an air-circulated oven at 150 °C, resulting in transparent homogeneous dark orange films with a thickness around 150 μm. Films of pure polymerized linseed oil **pLO** were prepared in a similar fashion. Model paint samples for zinc (**ZnO-LO**) or lead (**Pb_3O_4-LO**) were made by grinding ZnO and Pb_3O_4 with cold-pressed untreated LO in a 1:1 (w/w) ratio (zinc) and 2.75:1 (w/w) ratio (lead) to a smooth paste with mortar and pestle. The wet sample thickness was 190μm and the samples were dried at 60 °C in air for 7 days. For all measurements, 5 × 5 mm squares of the films were cut and lifted off the glass support. The thickness of each sample was measured with a digital micrometer accurate to 1 μm.

Analytical methods ATR-FTIR spectra were measured on a Perkin-Elmer Frontier FT-IR spectrometer fitted with a Pike GladiATR module that included a heated top plate and a diamond ATR-crystal ($\varnothing$ = 3 mm). Spectra were recorded every 10, 30 or 60 s at 4 cm^{-1} resolution and averaged over 4 scans. During time-dependent measurements, the ATR module was flushed with nitrogen to ensure a constant background signal. In order to measure spectra of polymer samples while they were exposed to solvents or solutions, a custom built stainless steel cylinder was used as illustrated in Figure 3.13. The cell volume was sealed with two solvent resistant O-rings between the top plate and the pressure clamp of the ATR module. The polymer sample was covered by a $\varnothing$ = 10 mm porous sintered metal disk, and a small but constant pressure was applied to the polymer sample

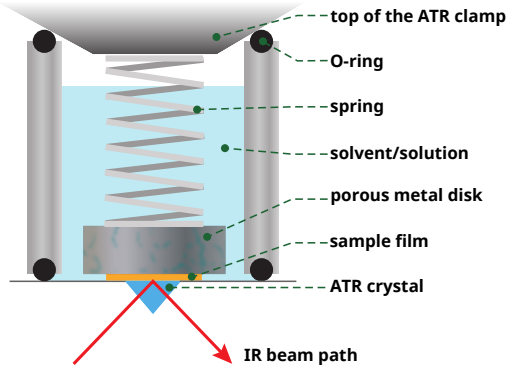

Figure 3.13 Illustration of the measurement cell used for time-dependent ATR-FTIR measurements of polymer films in contact with solvents or solutions. The spring provided a small pressure to keep a constant contact between the sample and the ATR-crystal as solvents swell the sample, while the porosity of the metal disk ensured unhindered diffusion of the solvent through the sample film.

by a spring placed between the pressure clamp of the ATR module and the porous disk. An inlet in the cylinder allowed for the addition of liquids to the sample chamber with a syringe. The inlet was kept sealed with parafilm during measurements to avoid solvent evaporation.

In all experiments, analytical grade solvents were used (analytical grade acetone contained up to 0.3 wt% water). In reactive measurements on pre-swollen films, the polymer sample was first swollen with 0.4 mL of pure acetone, and 1 mL of palmitic acid in acetone (20 mg/mL HPa) was added when the recorded IR spectra showed that the samples were fully saturated with acetone. For measurements with molten HPa, an adapted setup was used in which the stainless steel cylinder was replaced by a rubber septum ring. The porous metal disk was submerged in molten HPa for several minutes before a measurement, and then quickly placed on top of the sample that was pre-heated at 70 °C. Spectrum collection was started immediately after contact between the sample and HPa, after which the spring and rubber ring were put in place. The top plate of the ATR module was kept at 70 °C throughout these measurements.

X-ray diffraction X-ray diffraction (XRD) measurements were recorded with Cu Kα radiation at 1°/min on ca. 5 × 5 mm squares of polymer sample film taped to a silicon low-background sample holder.

Cross-sections Cross-sections were analysed with imaging-ATR-FTIR using a Perkin Elmer Spotlight 400 FTIR microscope equipped with a 16 × 1 pixel linear MCT array detector at 8 cm^{-1} resolution and a Perkin Elmer ATR Ge crystal accessory. Spectra were collected in the 750–4000 cm^{-1} range using an pixel size of 1.56 μm (diffraction limited

spatial resolution), an interferometer speed of 2.2 cm/s and averaging over 2 scans. Raw imaging ATR-FTIR data was processed using a custom Matlab script.

Illustration of two band isolation methods To integrate overlapping absorption bands accurately in the large datasets recorded during time-dependent measurements, data correction and integration algorithms were written in the Wolfram *Mathematica* software, which are available from the authors on request.

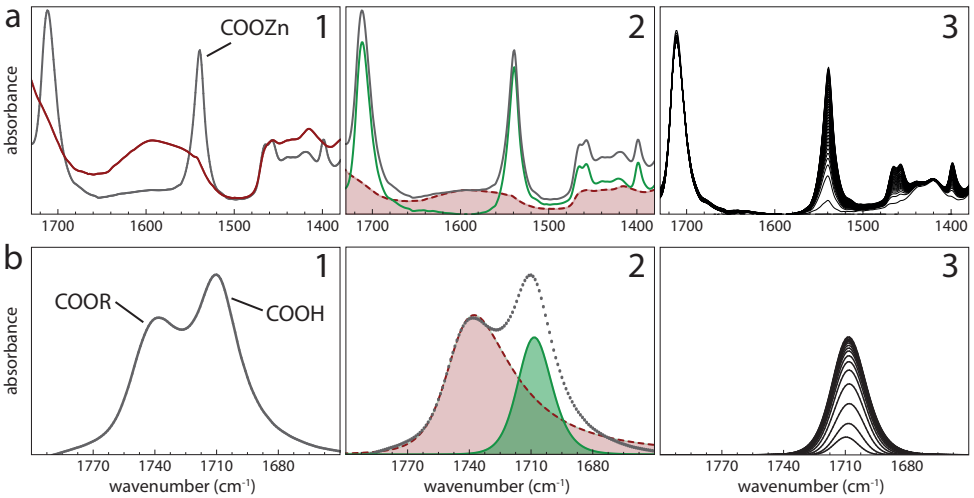

Figure 3.14 Illustration of two band isolation methods. **a**: For isolation of crystalline metal palmitate bands (shown for Zn here), the spectrum at $t = 0$ (red curve in 1) was scaled to each spectrum in a series (dashed line in (2)). The scaled $t = 0$ spectrum was then subtracted from each spectrum at $t > 0$ (green curve in 2), resulting a time-series of isolated crystalline metal carboxylate bands suitable for integration (3). **b**: For isolation of the COOH band (1), a combination of two constrained Pearson IV band shapes was fitted to each spectrum in a series (2), resulting in a series of fitted band shapes that could be integrated (3).

To obtain accurate time-dependent areas of the sharp metal carboxylate bands corresponding to crystalline lead palmitate (1510 cm^{-1}, shoulder at 1540 cm^{-1}) and zinc palmitate (1538 cm^{-1}), it was necessary to subtract the contribution of the partially overlapping broad amorphous metal carboxylate band from each spectrum (see Figure 3.14a). First, the spectrum of an unreacted film at $t = 0$ (shown in red) was scaled to each spectrum at later times by matching the intensities at a fixed position on the broad amorphous metal carboxylate band (COOZn, around 1600 cm^{-1}, where the contributions of surrounding bands are minimal). Subsequently, the scaled reference spectrum (dashed red curve) was subtracted from each spectrum in the series. The resulting isolated crystalline metal soap band (shown in green) could then be integrated by summing the intensity values in a fixed range that spanned most of the band.

During measurements of palmitic acid (HPa) diffusion into linseed oil polymer films,

the COOH band of HPa at 1710 cm^{-1} overlaps with the ester carbonyl band of linseed oil with a maximum at 1740 cm^{-1}. A stepwise profile fitting algorithm was applied to integrate the carboxylic band accurately (see Figure 3.14b). First, a Pearson type IV band shape[108] was fitted to the ester carbonyl band at $t = 0$ and all band parameters except band height were fixed. Second, the sum of two Pearson IV band shapes—one constrained ester carbonyl band and one unconstrained function—were fitted to the overlapping carbonyl bands in the last spectrum in the measurement series, after which all parameters except band height were also fixed for the COOH band. Finally, a combination of the two constrained band shapes was fitted to the entire spectrum series, and the time-dependent area of the COOH band could be calculated.

Acknowledgements

The authors thank Helena Willard (BSc. student, University of Amsterdam) for her contributions to the spectrum processing algorithms.